A Mathematical Model of the Volume, pH, and Ion Content Regulation in Reticulocytes

Application to the Pathophysiology of Sickle Cell Dehydration

Virgilio L. Lew, Carol J. Freeman, Olga E. Ortiz,* and Robert M. Bookchin*
*Physiological Laboratory, Cambridge University, Cambridge, United Kingdom; and *Department of Medicine, Albert Einstein College of Medicine, Bronx, New York 10461*

Abstract

We developed a mathematical model of the reticulocyte, seeking to explain how a cell with similar volume but much higher ionic traffic than the mature red cell (RBC) regulates its volume, pH, and ion content in physiological and abnormal conditions. Analysis of the fluxbalance required by reticulocytes to conserve volume and composition predicted the existence of previously unsuspected Na^+-dependent Cl^- entry mechanisms. Unlike mature RBCs, reticulocytes did not tend to return to their original state after brief perturbations. The model predicted hysteresis and drift in cell pH, volume, and ion contents after transient alterations in membrane permeability or medium composition; irreversible cell dehydration could thus occur by brief K^+ permeabilization, transient medium acidification, or the replacement of external Na^+ with an impermeant cation. Both the hysteresis and drift after perturbations were shown to depend on the pH_i dependence of the K:Cl cotransport, a major reticulocyte transporter. This behavior suggested a novel mechanism for the generation of irreversibly sickled cells directly from reticulocytes, rather than in a stepwise, progressive manner from discocytes. Experimental tests of the model's predictions and the hypothesis are described in the following paper. (*J. Clin. Invest.* 1991. 87:100–112.) Key words: reticulocyte • red cell volume/ion transport/model • sickle cell anemia

Introduction

The mean volume of reticulocytes exceeds that of mature red blood cells (RBCs)[1] by ~ 13% (1–5), but their ionic traffic is ~ 10-fold that of RBCs (6, 7). Since the ionic content of reticulocytes is similar to that of RBCs (7), it apparently remains fairly stable during maturation. The ion traffic across reticulocyte membranes must therefore remain balanced as it declines with maturation. The main ion transporters identified thus far in mammalian reticulocytes include the sodium pump (6, 7) and a ouabain- and bumetanide-insensitive, pH- and volume-sensitive K:Cl cotransport (6, 8–19).

In RBCs from persons homozygous for hemoglobin C (CC) or hemoglobin S (SS; sickle cell anemia), Brugnara et al. observed large K^+ flux components having the same features as those described for reticulocytes (9–11, 20, 21). The K^+ fluxes were largest in those density fractions richest in reticulocytes (9), suggesting a predominance in young cells (22, 23). The Cl^- dependence (19, 23, 24) and insensitivity to inhibitors, and pH and volume dependence, suggested that the K^+ transporter of human reticulocytes was identical to the K:Cl cotransport of sheep and goat reticulocytes (13), and that its presence may be a general feature of mammalian reticulocytes and young RBCs.

Despite intensive studies of the nature, timing, and synchrony of changes during erythroid cell maturation, little is known about how reticulocytes maintain osmotic stability and regulate pH and ion composition during their dynamic transformations. One basic question concerns the way reticulocytes balance their ionic traffic and prevent rapid dehydration via the K:Cl cotransport. Here we analyze these issues with the aid of a mathematical model that integrates the ion transport properties of the reticulocyte membrane with the known charge and nonideal osmotic behavior of hemoglobin (Hb), the main protein component of the reticulocyte cytoplasm. The results predict the existence of a large Na^+ gradient–dependent Cl^- entry mechanism, and show that, unlike mature RBCs (25), minor and even transient perturbations of pH and K^+ permeability may trigger large and irreversible changes in the volume, pH, and ion content of reticulocytes, and consequently in the mature cell product. The reticulocyte is thereby particularly vulnerable to abnormal permeabilizing events in the circulation, such as those associated with the intracellular polymerization of Hb S in more mature SS RBCs. Consideration of the possible effects of K^+ permeabilization of SS reticulocytes led us to formulate a working hypothesis on the formation of irreversibly sickled cells (ISCs) and other dense SS cells directly from a subpopulation of reticulocytes that had been permeabilized in the circulation.

Theoretical considerations. At physiological external pH, the K:Cl cotransport of human reticulocytes mediates a KCl efflux that varies widely, from 4 to 20 mmol/liter cells per h in reticulocyte-rich SS RBC fractions from different donors (9, 10). We wish to elucidate how a cell with such a powerful K:Cl cotransport regulates its volume, pH_i, and ion content, and the extent and manner in which its responses to physiological or experimentally induced changes differ from those of mature

A preliminary report of portions of this work was published in abstract form (1988. *Clin. Res.* 36:567A).

Address correspondence to Dr. Robert M. Bookchin, Department of Medicine, Rm. 913U, Albert Einstein College of Medicine, 1300 Morris Park Avenue, Bronx, NY 10461.

Received for publication 28 August 1989 and in revised form 12 June 1990.

1. *Abbreviations used in this paper:* CC, homozygous hemoglobin C disease; Hb, hemoglobin; ISC, irreversibly sickled cell; lcw, per liter cell water; loc, per liter original cells, or per 340 g hemoglobin; loch, per liter original cells (or per 340 g hemoglobin) per hour; RBC, red blood cell; SS, homozygous hemoglobin S disease, or sickle cell anemia.

J. Clin. Invest.

0021-9738//91/01/100/13 $2.00
Volume 87, January 1991, 100–112

RBCs. In formulating the basic properties of such a cell for the purpose of model simulations, we used a value of 15 mmol/loch for the K:Cl-mediated fluxes (9), setting aside issues of heterogeneity or decay rates of K:Cl transport among reticulocytes. If unbalanced, such a flux could shrink the cells by 20% or more in about an hour. Since reticulocyte volume is reduced by only ~ 10–15% over 2–3 d as the cells mature, either the K:Cl cotransport decays within hours in the circulation, or else high K:Cl reticulocytes must be in a balanced quasi-steady state.

A major question thus arises as to how the fluxes through the K:Cl cotransporter are balanced (Fig. 1). For K^+, the only uphill pathway is through the Na^+ pump; to bring in the 15 mmol/loch of K^+ lost from the cell via the K:Cl cotransport, it must pump out at least 22.5 mmol/loch of Na^+. Therefore, Na^+ influx in reticulocytes must also be much larger than the 2.5–3 mmol/loch found in mature RBCs. Increased Na^+ traffic in reticulocytes has been documented by Wiley and Shaller (7), but the pathways remain unknown.

For Cl^-, the balancing influx may be mediated either by transporters unique to reticulocytes or by those residually present in mature RBCs. The latter include three known Cl^- transport pathways: the anion exchange carrier (26–30); an electrodiffusional pathway (inhibitable by the same agents and to a similar extent as the carrier, and therefore considered a slippage through the carrier [31, 32]); and the K:Na:2Cl cotransporter (16, 33–38). Net Cl^- entry through any of these pathways requires a suitable gradient: a transmembrane hydroxyl or bicarbonate concentration ratio larger than that of Cl^- for the anion exchange carrier; a membrane potential that is depolarized, relative to the Cl^- equilibrium potential, for the diffusional pathway; or an intracellular $[K][Na][Cl]^2$ product lower than that in the outside medium, for the K:Na:2Cl cotransport.

In mature RBCs the K:Na:2Cl cotransport is at equilibrium and mediates no net fluxes (25, 35, 38); in the absence of evidence that reticulocytes have lower concentrations of Cl^-, Na^+, or K^+, it cannot be arbitrarily assumed that a driving gradient exists for net fluxes through a K:Na:2Cl cotransport. In addition, bumetanide, a known inhibitor of the K:Na:2Cl cotransport (34), failed to cause reticulocyte shrinkage (39). Mediation of net Cl^- entry by K^+-linked transport is therefore doubtful and not analyzed further.

Three other possibilities for net Cl^- entry, through familiar transport mechanisms that may operate in reticulocytes, are illustrated in Fig. 2: (*a*) Na^+ entry through a diffusional channel depolarizes the membrane relative to the Cl^- equilibrium potential, driving Cl^- in via conductive pathways (option 1, referred to as O1 below); (*b*) electroneutral Na:Cl cotransport (option 2, O2); and (*c*) Na^+ entry via a neutral Na:H exchange (40–43) generates an inward proton concentration gradient that drives Cl^- in through the Jacobs–Stewart mechanism, functionally equivalent to a H:Cl cotransport (25, 44, 45) (option 3, O3).

With each option, the energy for Cl^- entry is derived directly or indirectly from the Na^+ gradient; therefore, reticulocytes with high K:Cl-mediated fluxes ought to be critically dependent on the external Na^+ concentration to maintain a steady (or only slowly decreasing) cell volume. In that case, isotonic replacement of external Na^+ by an impermeant cation should dehydrate high K:Cl cells much faster and to a larger extent than mature RBCs, as described in Results. This prediction would be easy to test if a suitable, fully impermeant monovalent cation were available.

The behavior of cells with each of the three optional strategies illustrated in Fig. 2 will be analyzed separately below. One

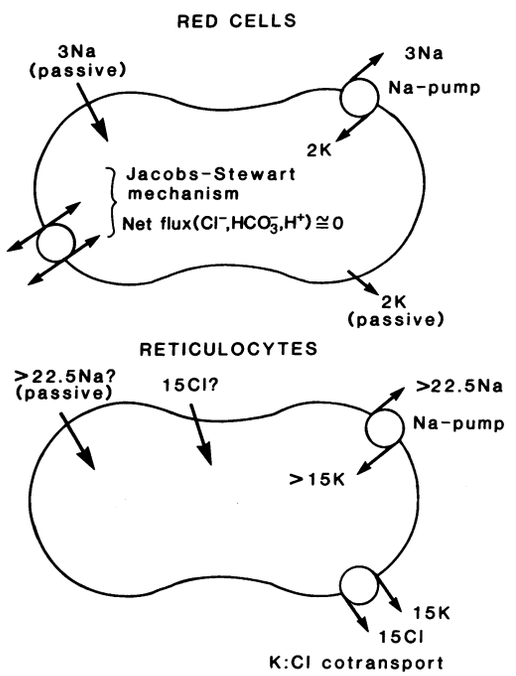

Figure 1. Ion traffic across the cell membrane: comparison between reticulocytes and mature RBCs. A large capacity K:Cl cotransport, active in reticulocytes but not in mature RBCs, mediates net K^+ and Cl^- efflux of 15 mmol/loch. Since the reticulocyte ion content does not change appreciably during maturation, alternative transporters must provide the balancing fluxes. Of these, only the Na^+ pump is known, whose activity in reticulocytes, more than sixfold that in RBCs, could account for the required K^+ influx. The corresponding pathways for the large inward Na^+ and Cl^- flux components required for overall ion balance have yet to be identified.

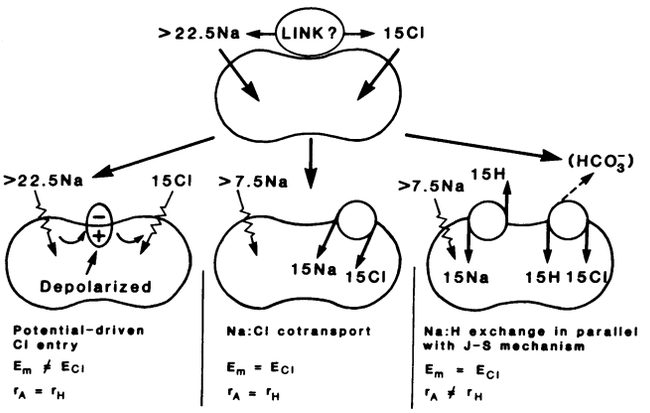

Figure 2. Alternative transport pathways for balancing net Na^+ and Cl^- entry in reticulocytes. The three mechanisms considered in the simulations reported here are shown diagrammatically, and are referred to henceforth as option 1 (O1), a potential-driven Cl^- entry; option 2 (O2), an electroneutral Na:Cl cotransport; and option 3 (O3), a Na:H exchange in parallel with Cl:H cotransport through the Jacobs–Stewart mechanism.

or more of these options may be expressed in different cells or in the same cell, but analysis of mixed options would be justified only if experiments eventually prove that more than one pathway mediates compensatory Cl^- influx in the same cell.

The mathematical model, glossary of symbols, and computation strategy are detailed in the Appendix. In the next section we report and analyze the result of simulations performed with the three model options defined here.

Results

Relation between membrane potential and diffusional Na^+ and anion permeabilities in a model with potential-driven net anion influx (O1 model). Fig. 3 shows the relations predicted by the O1 model between the reference state value of the membrane potential, and the values of the diffusional Na^+ and anion permeabilities. The results indicate that if the diffusional anion permeability of reticulocytes were similar to that of mature RBCs, e.g., $\approx 0.25\ h^{-1}$ (26), the membrane potential of reticulocytes would have to be less negative than with RBCs. If, on the other hand, the membrane potential of reticulocytes were in the normal range for RBCs (−8 to −15 mV), the diffusional anion permeability would have to be 5–50-fold higher than that of mature RBCs. Experimental measurement of membrane potential and Cl^- permeability in reticulocytes may thus help resolve whether or not Cl^- entry is driven by membrane potential.

Effect of external Na^+ replacement and low pH on cell volume. In the simulations of Fig. 4 we investigated the effects of maneuvers designed to alter the volume of reticulocytes and RBCs. The purpose of this was to compare responses predicted by reticulocyte and red cell models, and to try to design simple experimental procedures to separate mature RBCs from cells with transport features attributed to reticulocytes.

Fig. 4 *a* shows the predicted effects on the relative cell volume of RBCs and reticulocytes of replacing 120 mM external Na^+ with an impermeant monovalent cation such as *N*-methylglucamine. The predicted volume changes for the three reticulocyte model options are almost identical. The models predicted that reticulocytes would shrink at a much faster rate than mature RBCs, so that within 2 h their volume would be less and their density greater than those of RBCs. This prediction is important because, if confirmed, it would (*a*) demonstrate the postulated role of Na^+-dependent anion transport in short-term volume regulation by providing the Na^+ + anion fluxes needed to balance net K + Cl^- loss through the K:Cl cotransporter; (*b*) allow identification of young cells with transport properties of reticulocytes, regardless of whether they retain reticular structures; and (*c*) provide a method for separation and enrichment of reticulocytes, or of cells with residual transport properties of reticulocytes, from mixed cell populations.

Fig. 4 *b* shows the predicted effects of medium acidification. The resulting cell acidification protonizes negative charges of impermeant cell anion and causes secondary cell swelling as diffusible anions enter to restore electroneutrality. In reticulocytes, but not in mature RBCs, stimulation of the K:Cl-mediated fluxes by low pH_i quickly overrides the swelling effect of fixed charge protonation, resulting in cell shrinkage (O1 and O2 in Fig. 4 *b*). As anticipated, RBCs swell in the conditions simulated in Fig. 4 *b* by ~ 5% in the first few minutes. Fig. 4 *b* shows that the effects of low pH for option 3 models may differ from those with options 1 and 2. The Na:H exchanger was defined with a steep stimulatory effect of reduced cell pH (40, 46) similar to that defined for the K:Cl cotransport (see Eq. 1a in Appendix). When both of these systems are similarly stimulated by low pH_i, the net NaCl gain through the combined operation of the Na:H and anion exchangers exceeds net KCl loss through the K:Cl cotransport, and the cells swell. At first, medium acidification reduces the driving gradient, causing a transient depression of net Na influx through the Na:H exchanger (too brief to be seen in the figure). But as soon as the cells begin to acidify via the Jacobs–Stewart mechanism, proton efflux through the Na:H exchange increases both by direct pH_i stimulation of the exchanger and by elevation of the internal proton concentration. Without direct stimulation, the increase due to elevation of the proton concentration per se is not enough to prevent net salt loss and dehydration, and the O3 model behaves more like the O1 and O2 models (Fig. 4 *b*). These results indicate that a Na:H exchanger capable of balancing cation fluxes in steady state would not prevent acid-induced dehydration of O3 reticulocytes unless it were directly stimulated by low pH_i.

The curves in Fig. 4 *c* compare the predicted dehydration rates of O1 reticulocytes induced by Na^+ replacement, decreased external pH, or both. The initial dehydration rate in-

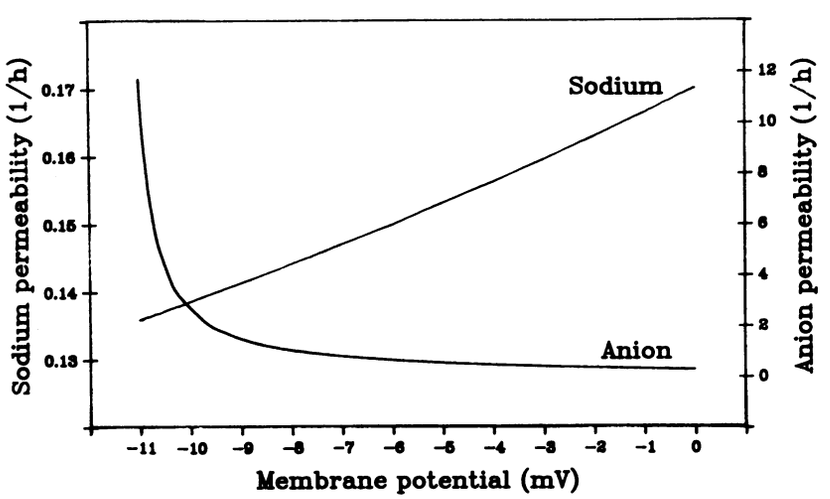

Figure 3. Relation between membrane potential and Na^+ and Cl^- (anion) electrodiffusional permeabilities in a reticulocyte model with potential-driven Cl^- (A^-) entry (option 1). In this option, the two equations for the electrodiffusional Na^+ and anion fluxes ($\phi_{Na}{}^G$ and $\phi_A{}^G$) link the three unknowns required for the computation of the reference state, membrane potential, and the diffusional permeabilities of Na^+ and anion (E, $P_{Na}{}^G$, and $P_A{}^G$; see Appendix). The computing strategy sets the E and derives $P_{Na}{}^G$ and $P_A{}^G$. The diffusional Na^+ permeability in all reticulocyte model options exceeds that of mature RBCs by at least two orders of magnitude ($\approx 0.15\ h^{-1}$ compared with $\approx 0.0015\ h^{-1}$ [25]).

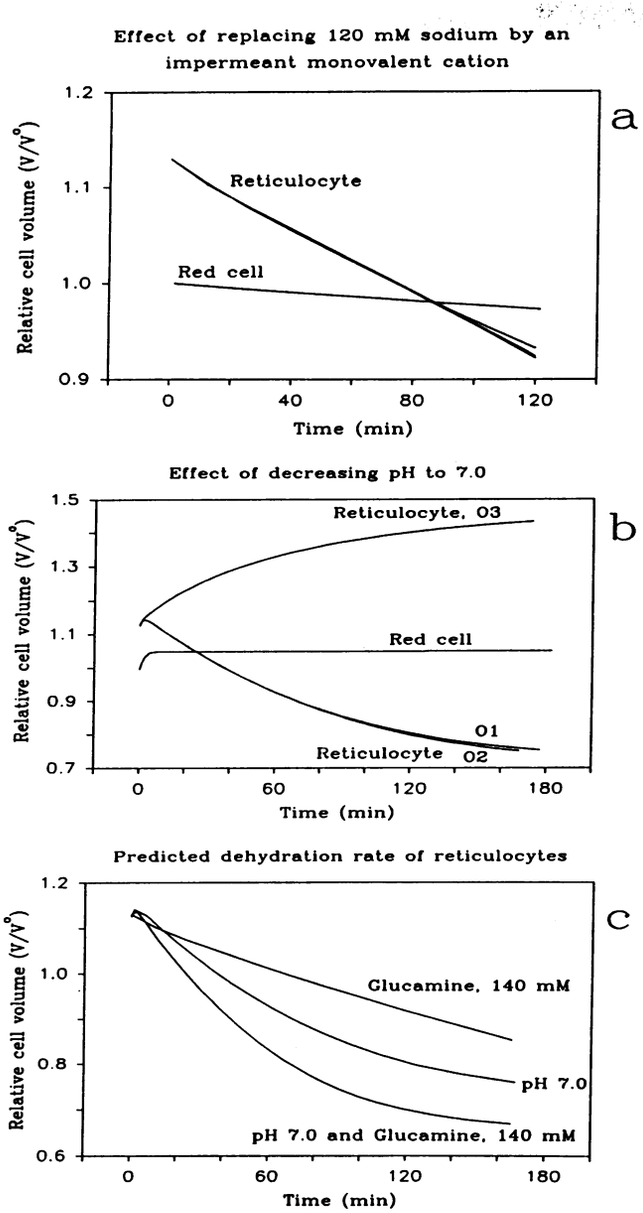

Figure 4. Predicted effects of Na^+ replacement and of low pH in the suspending medium on the relative cell volume of reticulocytes. For the precise definition of relative cell volume see "Cell water" section in Appendix. (*a*) Effect of replacing 120 mM Na^+ with an impermeant monovalent cation (represented by "glucamine"): comparison between reticulocytes (all three options coincide) and RBCs. The RBC changes were simulated with the integrated RBC model of Lew and Bookchin (25) using a reference state value for V_W of 0.75 lcw/loc (relative volume = 1). (*b*) Effect of decreasing medium pH from 7.4 to 7.0. It is important to allow for the redistribution of protons between cells and medium in these simulations. With a hematocrit (Hct) of 10%, as in this figure, medium pH recovered from 7.0 to ~ 7.3 in all options within 2 h. If the pH of the medium is kept constant at 7.0 (by lowering the Hct, for instance), the initial dehydration rate is faster, but its extent is smaller because cell acidification reaches inhibitory levels for the K:Cl cotransport (not shown). Since the dehydrating effects of low medium pH may vary with the Hct, it is important to take it into account, or to clamp external pH, when designing experiments to test the effect of reduced medium pH on reticulocyte volume. (*c*) Comparison of dehydration rates induced by Na^+ replacement (140 mM), lowered pH, or both. Simulations with the O1 model.

duced by Na^+ replacement is slower than that induced by medium acidification. The reason for this difference is that Na^+ removal exposes, at most, an unbalanced Cl^- efflux of 15 mmol/loch through the K:Cl cotransport, whereas low pH_i can stimulate an excess KCl efflux over NaCl influx of > 60 mmol/loch. When low pH_i is combined with Na^+ replacement, the dehydrating effects are initially additive, but in each case tend to level off, primarily as a result of ion gradient dissipation. (With Na^+ replacement alone, this leveling off occurs after 4–5 h, and is not seen in the figure.)

The stability of reticulocytes following transient perturbations. The time course of reticulocyte variables following transient perturbations is simulated in Fig. 5, after a 30-s increase in K^+ and anion permeabilities, and in Fig. 6, with a reversible change in medium pH from the reference state value of 7.4 to 6.5 (Fig. 6 *a*) or to 8.5 (Fig. 6 *b*), for 10 min. In these simulations the variables shown changed by < 7% during the period of the perturbation. The results show a fundamental difference between the behavior of the O3 model, in which all variables returned to near reference state values, and those of the O1 and O2 models, where variables drifted further from the initial displacements towards new steady states. However, if the pH_i dependence of the K:Cl cotransport was removed, no drift occurred and all variables returned to reference state values (not shown) as those of the RBC model always do (25). Thus,

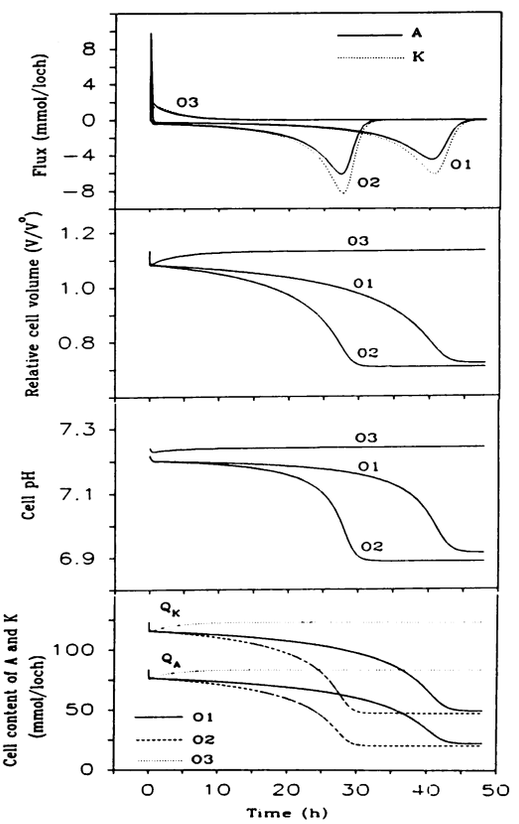

Figure 5. Predicted effects of a 30-s transient increase in K^+ and Cl^- (A^-) permeabilities on variables of the reticulocyte model, options 1–3. The K^+ permeability was increased to 10 h^{-1} and the Cl^- (A^-) permeability to 50 liters/h (47, 60). The variables reported (see plot ordinates) were, from top to bottom, net fluxes of K^+ and Cl^- (A^-), relative cell volume, cell pH, and K^+ and Cl^- (A^-) content of the cells.

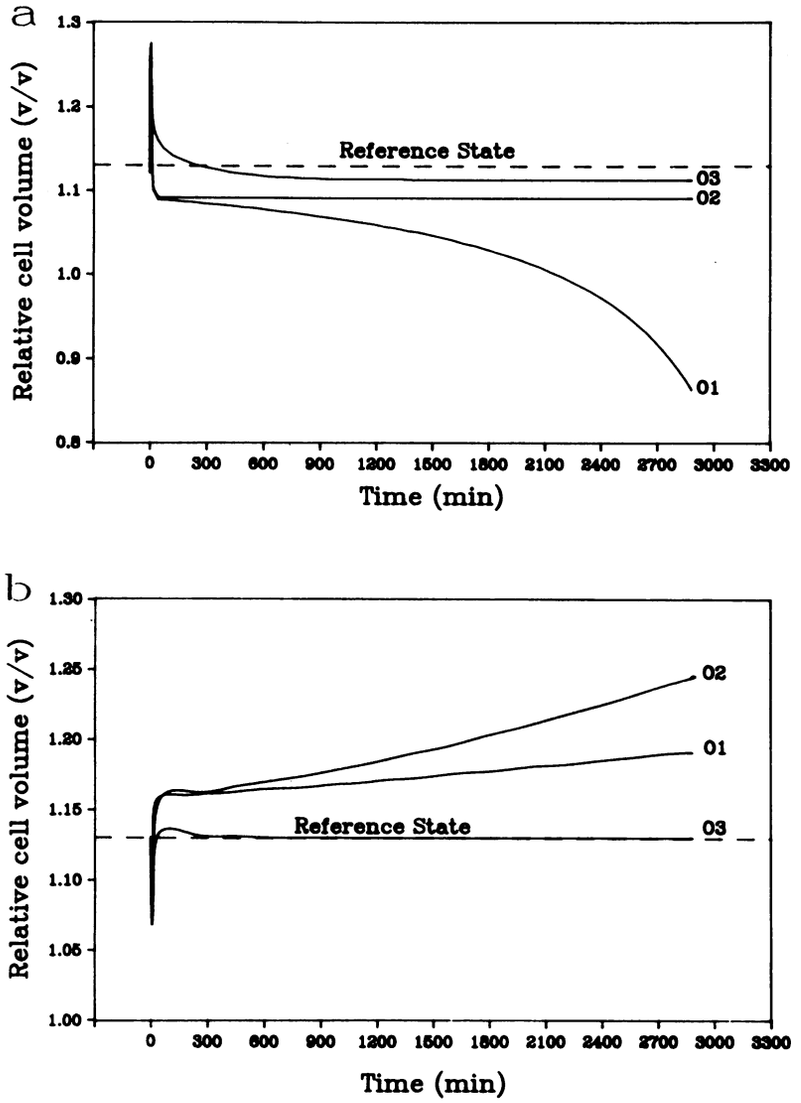

Figure 6. Predicted effects of transient external pH changes on relative cell volumes (reticulocyte model, options 1–3). pH changes were to 6.5 (*a*) and to 8.5 (*b*) for 10 min. The dashed lines represent the relative cell volume in the reference state.

dependence of a major cell transporter on pH_i may generate drift of the variables. Even in the absence of such drift, the new steady states after transient perturbations differed from the original reference state (see O2 and O3 models in Fig. 6 *a* and O3 in Fig. 6 *b*). Hysteresis and drift of variable values after transient perturbations of reticulocytes are therefore predicted responses resulting from the pH_i dependence of their K:Cl cotransport. Note that the duration of the latent period between the perturbation and the onset of dehydration, as well as the rate at which the variables change to dehydrated state values, may vary dramatically. Such variations may range over minutes or days, depending on the nature, extent, and reiteration of the transient perturbations, and on the V_{max}, kinetics, and relative decay rates of the various transporters. Therefore, the delays shown in Figs. 5 and 6 should be considered qualitative.

Before considering the implications of the hysteretic responses in Figs. 5 and 6, we will analyze their mechanism. In all instances where drift is observed, study of the residual fluxes after the transient perturbations reveals a mismatch between the rates of net Cl^- efflux through the K:Cl cotransporter and net Cl^- influx through the Na^+-dependent pathways. For instance, after a transient K^+ permeabilization, the membrane potential rapidly returns to normal, as do the Na^+ fluxes and Na^+-dependent Cl^- fluxes. But the cell acidification that resulted from K^+ permeabilization and initial dehydration (47; see below) continues to stimulate the K:Cl cotransporter, and the K^+ and Cl^- fluxes persistently exceed the reference state values. This causes slow and sustained dehydration. As dehydration proceeds, the cells are further acidified, progressively stimulating the K:Cl cotransport in a positive feedback loop. The process accelerates until the driving gradients collapse, and the inhibitory effects of cell shrinkage and very low pH reduce the K:Cl cotransport flux to near zero, in a final dehydrated steady state (Fig. 5). Essentially the same kind of imbalance between net Cl^- efflux and influx underlies the drifts predicted after low pH transients (Fig. 6).

The imbalance is much smaller in the O3 than in the O1 and O2 models, mainly because the proton fluxes through the Jacobs–Stewart mechanism in O3 are partly balanced by H fluxes through the Na:H exchanger. The cell pH shifts are therefore smaller in O3, providing less stimulation or inhibition of the K:Cl cotransport by pH_i. The corresponding transients are smaller and occur later (see below and Fig. 7) than

with O1 and O2, and the post-recovery steady states are closer to the reference state.

In conclusion, the simulations in Figs. 5 and 6 indicate that the pH_i dependence of the K:Cl cotransport makes reticulocytes unstable in the sense that they may respond to transient perturbations with drift or hysteresis. These effects are much larger in O1 and O2 models than in O3 models. Their extent in real cells will depend on the true kinetics and size of the main fluxes; if, for instance, younger or prematurely released reticulocytes had much higher fluxes than 2–3-d-old cells, they would be more vulnerable to transient perturbations. The simulations in Fig. 5 suggest that repeated K^+ permeabilization in the circulation would dehydrate reticulocytes more than mature RBCs. The possible relevance of this prediction to mechanisms of sickle cell dehydration will be considered in the Discussion.

Effects of sustained K^+ permeabilization of reticulocytes. K^+ permeabilization was shown to dehydrate and acidify mature RBCs suspended in low K^+, plasmalike media (25, 47). The simulations in Figs. 7 and 8 show that the predicted effects

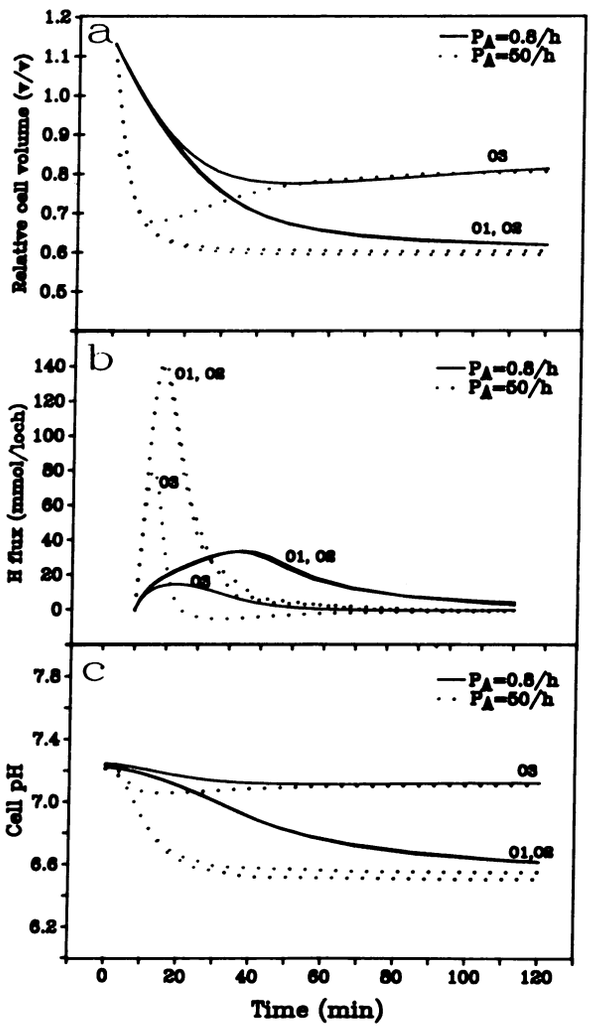

Figure 7. Predicted effects of a sustained increase in K^+ permeability, with or without a concomitant increase in Cl^- (A^-) permeability, on variables of the reticulocyte model, options 1–3. Variables reported are shown in plot ordinates. Anion permeabilities (P_A) are shown.

of K^+ permeabilization are qualitatively similar for both reticulocytes and RBCs. The cells first lose isotonic KCl, in which the effluent Cl^- concentration ($\approx$ 150 mM) exceeds that of cell water ($\approx$ 100 mM). The isotonic KCl loss therefore dilutes cell Cl^-, increasing the inward Cl^- concentration ratio. The response of the Jacobs–Stewart mechanism to match the outward proton concentration ratio results in cell acidification and medium alkalinization.

Fig. 7 *b* shows that the proton shifts in O1 and O2 reticulocytes are similar in timing and extent to those observed in RBCs (25, 47). In O3 the proton fluxes peak earlier than those of O1 and O2, but the peaks are small and brief. The secondary effects of these flux differences on relative cell volumes are shown in Fig. 7 *a*. The initial volume changes are similar in all models, but in O3 the volume either falls less than in O1 and O2, or recovers later to a less dehydrated steady value. As with RBCs (25), the increased anion flux declines faster than the increased K^+ flux (Fig. 8). In RBCs this difference corresponds entirely to the H^+ flux, but in reticulocytes the Na^+ flux participates in the balance, particularly in O3 models, where the dehydration-induced outward proton gradient drives a net Na^+ influx through the Na:H exchanger. As a result of the corresponding retention of anion, there is less acidification to stimulate the K:Cl cotransport, and therefore also less dehydration (or earlier rehydration, as in Fig. 7 *a*) than in O1 and O2 models.

Discussion

Analysis of the design and behavior of alternative reticulocyte models (O1, O2, and O3) suggests that reticulocytes, unlike mature RBCs, need Na^+-dependent anion influx transporters to maintain volume stability, and respond to transient perturbations of cell volume or pH with hysteresis and further drift of ion content, pH, and cell volume. These features can be attributed to the large-capacity pH_i- and volume-dependent K:Cl cotransport, by mechanisms described in the previous section. The intrinsic instability and vulnerability of reticulocytes is thus the result of the activity of a transient transporter. This points out a potentially more general property of transitional cells, or of cells in transitional developmental stages. In such states, the transport systems that normally secure the high osmotic stability of mature cells (25, 48) may be overridden by transient transporters required for specific developmental needs (49). This would render transitional cells more vulnerable than the mature cell products to permeabilizing membrane injuries or environmental changes.

We consider now the possible relevance of the model predictions to the pathophysiology of conditions such as sickle cell anemia, in which dehydrated RBCs appear in the circulation. The dense SS cell fractions, which contain a high proportion of ISCs, are thought to play an important role in both the hemolytic anemia (50) and the vaso-oclusive episodes (51) in patients with sickle cell anemia. Much effort has therefore been directed towards understanding the mechanism of cell dehydration. Two main mechanisms considered previously were activation of Ca^{2+}-sensitive K^+ channels (52–56), and Na^+ pump–mediated dehydration following sickling-induced balanced Na^+/K^+ dissipation (55, 57). It was recognized that if the cells acidified in the circulation, net KCl loss and dehydration could be mediated by a K:Cl cotransport (9, 22), as recently demonstrated in vitro with SS RBCs (12, 58). How-

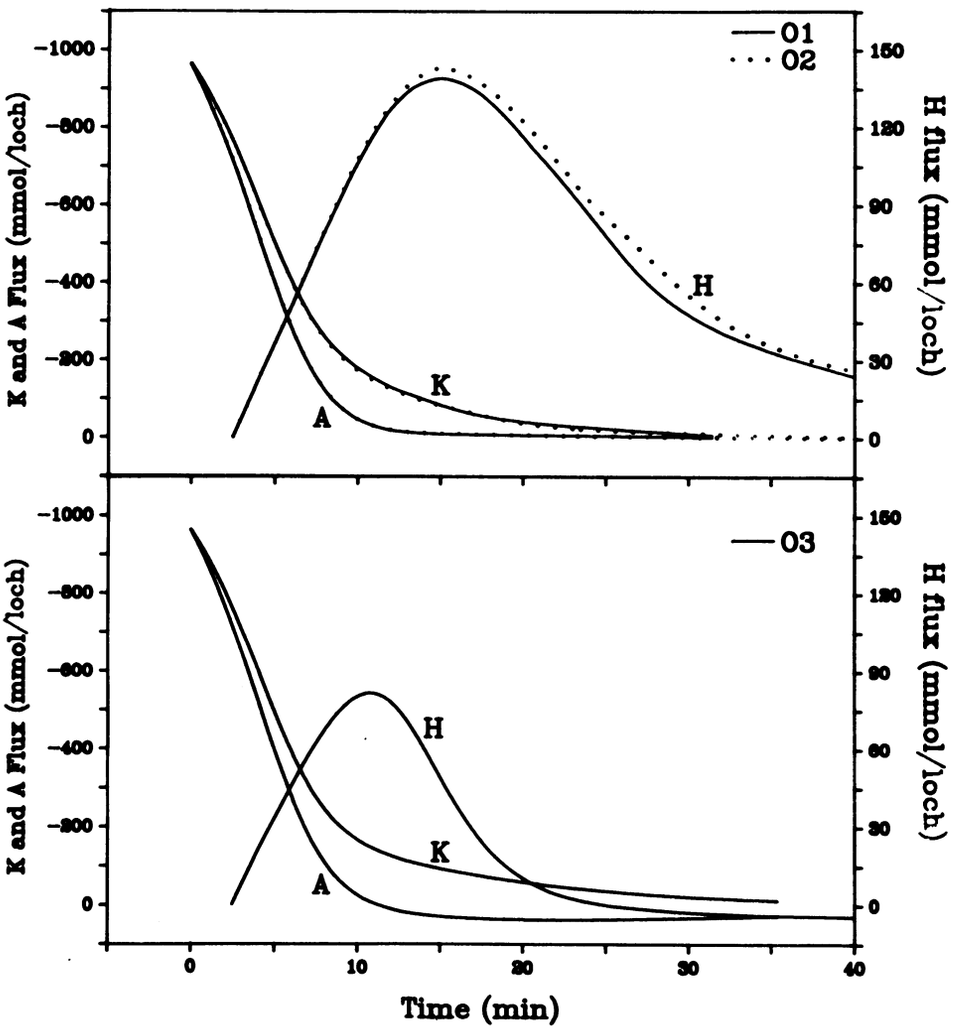

Figure 8. Relation between the fluxes of K^+, Cl^- (A^-), and protons in K^+-permeabilized reticulocytes. Model options 1 and 2 are shown in the top panel, and option 3 is shown in the bottom panel. Note the separate ordinate scales for K^+/A^- and H^+ fluxes on the left and right, respectively.

ever, the actual role of this transport pathway in SS cell dehydration in vivo remains unclear.

Together with the evidence for the presence of a K:Cl cotransport in reticulocytes, two additional observations provide clues for an alternative hypothesis on the possible mechanism of ISC formation. The first observation, by Bertles and Milner (59), indicated that ISCs represent a population of cells much younger than most of the discocytes of the same blood sample. The second, more recent observation concerns the acidification of K^+-permeabilized RBCs suspended in low K^+ media, which was first predicted by the RBC model and later confirmed experimentally with normal RBCs (25, 47). As shown here in Figs. 7 and 8, cell acidification following K^+ permeabilization is also predicted for reticulocytes.

The new hypothesis proposes that ISCs and other dense SS cells are generated primarily from reticulocytes directly, rather than from discocytes, by the following mechanism (see Fig. 9). Either before or after release into the circulation, some reticulocytes would become slightly acidified, either directly, by a low environmental pH, or indirectly, by sickling-induced Ca^{2+} permeabilization followed by K^+ channel activation and cell dehydration. The lowered pH_i would stimulate the K:Cl cotransport, causing KCl and water efflux, with further dehydration and cell acidification in a positive feedback loop, towards a highly dehydrated state. This predicted behavior, demonstrated here by the reticulocyte model, that only one or few initial events providing minimal acidification may suffice to trigger irreversible dehydration in SS reticulocytes, had not been considered before. The model also shows that for a K:Cl cotransport with the kinetic properties described in SS and CC cells (9–11, 56), inhibition by cell shrinkage is not sufficient to counterbalance stimulation by low pH_i.

There are thus two possible triggers of the K:Cl cotransport by low pH_i: either plasma acidification or sickling-induced Ca^{2+} permeabilization. Plasma acidification may at first appear more likely (56) because circulatory acidification is a common physiological event, and also because in reticulocytes the relatively low cell Hb concentration might not generate enough polymer on deoxygenation to permeabilize the membrane. However, the increased total calcium content of SS cells from all density fractions documents past episodes of Ca^{2+} permeabilization in the circulation (51, 52, 60, 61), whereas dehydration by circulatory acidification remains hypothetical. If plasma acidification can dehydrate reticulocytes, dense RBCs should appear in the blood of patients with chronic uncompensated acidosis, at a rate of at least 1% per day, and to a lesser extent in athletes, in whom local metabolic acidosis in the muscle vasculature is to be expected; to our knowledge this has not yet been investigated. The following paper (39) demonstrates that sickling causes permeabilization of SS reticulo-

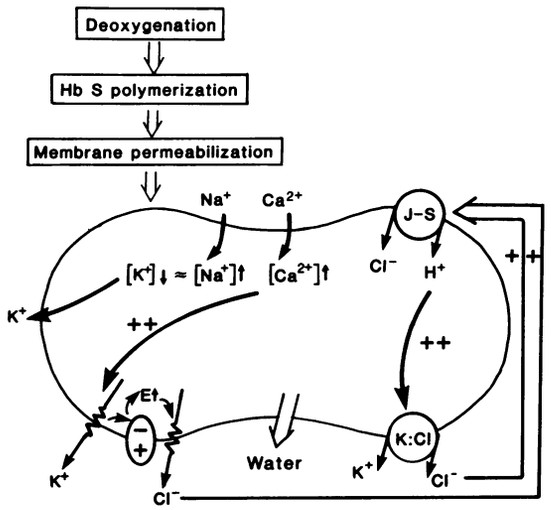

Figure 9. Working hypothesis on the mechanism of generation of ISCs directly from SS reticulocytes. Even small and brief acidification of cells with the transport properties of SS reticulocytes may initiate an irreversible process of further acidification and dehydration. Cell acidification may be triggered by circulation through capillary beds with low pH or, as shown on the diagram, by deoxygenation-induced sickling. The latter is assumed to permeabilize the cell membranes to cations, as with SS discocytes, thereby producing increased calcium influx, elevated $[Ca^{2+}]_i$, K^+ channel activation, dehydration, and acidification. Acidification, in turn, stimulates KCl efflux through the pH_i-sensitive K:Cl cotransport, activating the positive feedback cycle which leads to further cell dehydration and acidification.

cytes, with much more rapid and extensive Ca^{2+}-dependent net cation loss and dehydration than in mature RBCs. Depending on the incidence of sickling-related events during maturation, and on the susceptibility of the reticulocytes, they could therefore evolve into either discocytes or ISCs (or other dense forms). The results in Figs. 5 and 6 show that this mechanism is theoretically feasible, since brief K^+ and Cl^- (62) permeabilization (Fig. 5, O1 and O2), or transient extracellular acidification (Fig. 6, O1), is sufficient to trigger irreversible and accelerating dehydration. By contrast, in mature RBCs such acidification would cause only reversible swelling, and a similar extent of K^+ permeabilization would result only in transient, minor dehydration (25). The proposed hypothesis could also account for at least some of the abnormally dense SS reticulocytes found among discocytes in all density fractions: these may represent transitional stages to ISCs, and may thus exhibit characteristic differences from discocytes in the same density fraction, and similarities with dense SS cells and ISCs.

Appendix

Mathematical Model of the Volume, pH, and Ion Content Regulation of Reticulocytes

Glossary of symbols

For simplicity and for consistency with the nomenclature used for the integrated RBC model (25), no distinction will be made between Cl^- and any other highly permeant anion (A^-, see below). The K:Cl and Na:Cl cotransports will therefore be described as K:A and Na:A, respectively, in the corresponding symbols, and referred to interchangeably as K:Cl or K:A, and Na:Cl or Na:A. The implied identity $Cl^- = A^-$ is valid for all the conditions and simulations analyzed in this paper; for modeling cell behavior in the presence of permeant anions other than Cl^-, which are transported by the anion carrier but not by the cotransport systems, a clear distinction would be necessary.

Q_i	Amount of solute i in 1 liter of original packed cells (millimoles/loc)
$Q_{(\pm)}$	Net charge on impermeant cell ion (milliequivalents/loc)
C_i^c, C_i^m	Concentration of solute i in cell water (c) or in extracellular medium (m) (molar, M, for H^+ ions; millimolar, mM for all other solutes)
Subscript i	All solutes or any subset of solutes among Na, K, Mg, A, Hb, X, Y, B, HB, and H
Hb	Hemoglobin
A^-	Permeant anion
X	Impermeant intracellular anion, assumed to be nonprotonizable within pH; range explored in present simulations
Y(±)	Impermeant extracellular monovalent ion (gluconate, *N*-methylglucamine ["glucamine" in figures], or choline, for instance)
B	Impermeant extracellular H^+ buffer (Hepes-like, in the present simulations)
HB	Protonized form of extracellular H^+ buffer
K_B	Dissociation constant of extracellular H^+ buffer (molar)
pH^c, pH^m	Cell and medium pH, respectively
n_x, n_{Hb}	Mean net charge on X and Hb, respectively (equivalents/mole).
pI	Isoelectric pH of Hb
MCHC	Mean corpuscular Hb concentration (grams/deciliter packed cells)
a	Net negative charge on Hb when $pH^c = pI + 1$ (equivalents/mole); slope of the proton titration curve of Hb (63, 64)
f_{Hb}	Osmotic coefficient of Hb (iosmoles/mole)
b, c	Virial coefficients of linear and quadratic terms, respectively, in empirical equation for f_{Hb} (65)
V_W	Volume of cell water in 1 liter of original packed cells (liters/loc)
z_i, F, R, T, E	Valence of ion i, Faraday constant, gas constant, absolute temperature, and membrane potential (millivolts), respectively
σ_i	Total flux of permeant solute i (millimoles/loc)

Partial flux component of solute i (millimoles/loc) through:

ϕ_i^P	The Na^+ pump (P)
ϕ_i^L	Low saturation facilitated diffusion carriers (L)
ϕ_i^G	Electrodiffusional constant-field channels (G)
ϕ_i^{HA}	H:A (HA) cotransport (represents the operation of The Jacobs–Stewart mechanism [25, 44, 45])
ϕ_i^{KA}	K:Cl (KA) cotransport
ϕ_i^{NaA}	Na:Cl (NaA) cotransport
ϕ_i^{NaH}	Na:H (NaH) countertransport
ϕ_{Na}^{Fmax}, ϕ_{Na}^{Rmax}	Saturated forward (F) and reverse (R) Na^+ fluxes through the Na^+ pump (millimoles/loch)
P_i^L, P_i^G	Permeability constant of solute i through facilitated diffusion (L) and electrodiffusional (G) pathways (h^{-1})
k_{HA}	Rate constants for the H:A (HA) cotransport
k_{KA}	Rate constant of K:A cotransport
n_{KA}, K_{KA}^H	Parameters of K:A pH dependence factor (Eqs. 1, 1a, 1b)
K_{KA}^V	Parameter of K:A volume dependence factor (Eq. 1b)

f^{H}_{KA}, f^{V}_{KA}	pH_i and volume dependence coefficients, respectively, of K:A cotransport
k_{NaH}	Rate constant of the Na:H exchange
Hct	Hematocrit, expressed as volume fraction of cells
Dt	Integration interval (hours)
f_{Dt}	Integration interval factor
DV_w	Change in the volume of cell water per unit original volume of cells during one integration interval (liters/loc)
DQ_i	Change in the intracellular amount of solute i per unit original volume of cells during one integration interval (millimoles/loc)
r_A, r_H	Ratio between external and internal permeant anion concentrations (r_A) or between internal and external hydrogen ion concentrations (r_H)

Superscripts (o, t, and t-Dt) on a variable indicate the value of that variable in the original reference steady state (o), at any subsequent time (t), or at the preceding computing time (t − Dt). The absence of a time-indicating superscript on any variable is equivalent to the superscript t.

Fundamental equations of the reticulocyte model

1. Isotonicity

$$f_{Hb}\cdot Q_{Hb} + Q_{Na} + Q_K + Q_{Mg} + Q_X + Q_A = V_w(C^m_{Na} + C^m_K + C^m_A + C^m_B + C^m_Y)$$

2. Initial electroneutrality

$$Q^o_{Na} + Q^o_K + 2Q_{Mg} - Q^o_A + n^o_{Hb}\cdot Q_{Hb} + n_X\cdot Q_X = 0$$

3. Nonideal osmotic behavior of Hb

$$f_{Hb} = 1 + b\cdot Q_{Hb}/V_w + c\cdot Q^2_{Hb}/V^2_w$$

4. H^+ buffer behavior of Hb

$$n_{Hb} = a(pH^c - pI)$$

5. Flux equations

$$\phi_{Na} = \phi^P_{Na} + \phi^L_{Na} + \phi^G_{Na} + \phi^{Co}_{Na} + \phi^{NaH}_{Na} + \phi^{NaA}_{Na}$$

$$\phi_K = \phi^P_K + \phi^L_K + \phi^G_K + \phi^{Co}_K + \phi^{KA}_K$$

$$\phi_A = \phi^G_A + \phi^{Co}_A + \phi^{HA}_A + \phi^{KA}_A + \phi^{NaA}_A$$

$$\phi_H = \phi^G_H + \phi^{HA}_H + \phi^{NaH}_H$$

6. Maintenance of electroneutrality

$$\Sigma(z_i\cdot\phi_i) = 0$$

7. Computation of transients

$$DQ_i = \phi_i\cdot Dt$$

8. Redistribution of permeant solutes between cells and medium

$$C^{m(t)}_i = C^{m(t-Dt)}_i\{[1 + Hct/(1 - Hct)]DV_w\} - [Hct/(1 - Hct)]DQ_i$$

Definitions

D1. $C^c_i = Q_i/V_w$

D2. $\phi_i = DQ_i/Dt$

D3. $C^{c,m}_H = \exp_{10}(-pH^{c,m})$

D4. $pH^{c,m} = -\log C^{c,m}_H$

D5. $r_A = C^m_A/C^c_A$

D6. $r_H = C^c_H/C^m_H = \exp_{10}(pH^m - pH^c)$

D7. $Q_{(-)} = n_{Hb}\cdot Q_{Hb} + n_X\cdot Q_X + 2Q_{Mg}$

D8. $DV_w = V^{(t)}_w - V^{(t-Dt)}_w$

D9. $DQ_i = Q^{(t)}_i - Q^{(t-Dt)}_i$

D10. Na^+ pump–mediated fluxes

Forwards: $\phi^{PF}_{Na} = -\phi^{Fmax}_{Na}\{C^c_{Na}/[C^c_{Na} + 0.2(1 + C^c_K/8.3)]\}^3 \times (C^m_K/(C^m_K + 0.1(1 + C^m_{Na}/18)))^2$

Reverse: $\phi^{PR}_{Na} = \phi^{Rmax}_{Na}\{C^c_K/[C^c_K + 8.3(1 + C^c_{Na}/0.2)]\}^2 \times \{C^m_{Na}/[C^m_{Na} + 18(1 + C^m_K/0.1)]\}^3$

Net: $\phi^P_{Na} = \phi^{PF}_{Na} + \phi^{PR}_{Na}$

$\phi^P_K = -\phi^P_{Na}/1.5$

D11. Carrier-mediated fluxes

$$\phi^L_i = -P^L_i(C^c_i - C^m_i)$$

D12. Jacobs–Stewart flux

$$\phi^{HA}_H = \phi^{HA}_A = -k_{HA}(C^c_A\cdot C^c_H - C^m_A\cdot C^m_H)$$

D13. Electrodiffusional fluxes

$$\phi^G_i = -P^G_i\cdot(z_iFE/RT)\cdot[C^c_i - C^m_i\cdot\exp(-z_iFE/RT)]/[1 - \exp(-z_iFE/RT)]$$

D14. $\Sigma C^m_i = C^m_{Na} + C^m_K + C^m_A + C^m_B + C^m_Y$

D15. $MCHC = (MCHC)^o\cdot(V^o/V)$

Table I. Parameters of the Reticulocyte Model

Parameter	Value	Units
a	$-1.00.10^{+1}$	meq/mmol
b	$6.45.10^{-2}$	—
c	$2.58.10^{-2}$	—
pI	6.85	—
K_B	$2.81.10^{-8}$	M
$K_{KA}{}^H$	$1.20.10^{-7}$	mM
$K_{KA}{}^V$	0.88	lcw/loc
k_{KA}	$7.95.10^{-3}$	liters/h^{-1}
$Q_{10}{}^P$	4.00	—
$Q_{10}{}^L$	2.00	—
$\phi_{Na}F_{max}$	$8.99.10^{+1}$	mmol/loch
$\phi_{Na}R_{max}$	$1.00.10^{+2}$	mmol/loch
$\phi_K{}^L$ (RS)	−2.00	mmol/loch
$\phi_K{}^G$ (RS)	−0.20	mmol/loch
$P_{Na}{}^L$	$2.24.10^{-2}$	liters/h^{-1}
$P_K{}^L$	$1.48.10^{-2}$	liters/h^{-1}
$P_K{}^G$	$1.83.10^{-3}$	liters/h^{-1}
$P_A{}^G$	2.65	liters/h^{-1}
k_{HA}	$5.00.10^{+7}$	liters/h^{-1}

	Value			
Parameter	Option 1	Option 2	Option 3	Units
n_X	−0.91	−0.91	−0.88	meq/mmol
k_{NaH}	0.00	0.00	$7.70.10^{+14}$	—
n_{KA}	$5.41.10^{+14}$	$5.41.10^{+14}$	$4.87.10^{+14}$	—
$P_{Na}{}^G$	0.14	$4.62.10^{-2}$	$4.62.10^{-2}$	liters/h^{-1}
k_{NaA}	0.00	$7.52.10^{-4}$	0.00	liters/h^{-1}
k_{NaH}	0.00	0.00	$3.79.10^{+7}$	liters/h^{-1}

Values common to each of the three options for net Cl^- entry considered in this paper are shown in the top section, while the bottom part shows those values that vary for the three options. Parameter values were set or derived as explained in Computation Strategy (Appendix).

Table II. Flux Components of the Reticulocyte Model, Option 1, in the Reference State

Fluxes (option 1) (mmol/loch)	Na	K	A	H
Na pump				
Forward	$-2.58.10^{+1}$			
Reverse	$1.55.10^{-2}$			
Net	$-2.58.10^{+1}$	$1.72.10^{+1}$		
Carriers	3.00	−2.00		
Electrodiffusional	$2.28.10^{+1}$	−0.20	$1.50.10^{+1}$	0.00
Jacobs–Stewart (ϕ^{HA})	—	—	0.00	0.00
K:A cotransport (ϕ^{KA})	—	$-1.50.10^{+1}$	$-1.50.10^{+1}$	—
Na:A cotransport (ϕ^{NaA})	0.00	—	0.00	—
Na:H exchange (ϕ^{NaH})	0.00	—	—	0.00
Total net flux	0.00	0.00	0.00	0.00

Options 2 and 3 have the same reference state flux components as above except for the following:

	Option 1	Option 2	Option 3
Na	$\phi^{G} = 2.28.10^{+1}$	$\phi^{G} = 7.80$ $\phi^{NaA} = 1.50.10^{+1}$	$\phi^{G} = 7.80$ $\phi^{NaH} = 1.50.10^{+1}$
A	$\phi^{G} = 1.50.10^{+1}$	$\phi^{G} = 0.00$ $\phi^{NaA} = 1.50.10^{+1}$	$\phi^{G} = 0.00$ $\phi^{HA} = 1.50.10^{+1}$
H	$\phi^{HA} = 0.00$	$\phi^{HA} = 0.00$	$\phi^{HA} = 1.50.10^{+1}$ $\phi^{NaH} = -1.50.10^{+1}$

The reference state fluxes through the K:Cl cotransport were set at 15 mmol/loch and all other fluxes were derived as detailed in Computation Strategy (Appendix). Specific differences between options 1, 2, and 3 are given in the bottom part of the table.

Computation strategy

As with previous non–steady-state models (25, 64), we first computed a reference steady state to represent physiological conditions; we then introduced a perturbation that simulates an experimental or physiological event, and followed the changes in model variables with time to obtain the transient behavior of the system.

The flux equations

In the integrated model of mature RBCs (25), all ion fluxes and flux parameters in the reference steady state were derived from the well-established equality of anion/proton ratios and from the Na^+/K^+ pump–mediated fluxes. Since the best documented ion transport system in reticulocytes is the K^+ efflux through the K:Cl cotransport, it was chosen as the basis from which the other ion fluxes in the integrated reticulocyte model would be derived. We used the data and experimental curves of Brugnara et al., as observed with reticulocyte-rich SS cell fractions (9, 10, 21), to set the size of the K:Cl-mediated fluxes in the reference state, and to define the kinetics, cell pH, and volume dependence of this cotransporter. Four parameters were needed for an adequate phenomenological fit of the experimental curves (9, 21), and no further refinement was considered justified. The following equation (Eq. 1) was used in the present simulations:

$$\phi_A^{KA} = \phi_K^{KA} = k_{KA} \cdot f_{KA}^{H} \cdot f_{KA}^{V} \cdot (C_K^m C_A^m - C_K^c C_A^c) \quad (1)$$

$$\text{where } f_{KA}^{H} = \exp - n_{KA}(C_H^c - K_{KA}^{H})^2 \quad (1a)$$

$$\text{and } f_{KA}^{V} = \exp - (K_{KA}^{V} - V_w)/K_{Ka}^{V}) \quad (1b)$$

The parameters are:

k_{KA}	rate constant of K:A cotransport
n_{KA}, K_{KA}^{H}	parameters of pH dependence factor
K_{KA}^{V}	parameter of volume dependent factor.

Eq. 1 states that the K^+ flux through the K:Cl cotransport is electroneutral and proportional to the concentration gradients of the transported ions. The proportionality factor is modified by pH_i and volume dependence coefficients (f_{KA}^{H} and f_{KA}^{V}, respectively), defined in Eqs. 1a and 1b. The experimentally observed curves (9–11) suggest that the effects of volume are weaker than those of pH_i, and this is reflected in the values derived for the corresponding coefficients. The pH_i coefficient f_{KA}^{H} (Eq. 1a) also provides for inhibition of the cotransport at pH_i values more acid than the maximum. The pH_i factor can vary between 0 and 1, and its reference state value was set at 0.15, since at physiological pH_i, f_{KA}^{H} is ~ 15% of maximal (9, 21). The cell pH at which the flux became maximal was ~ 6.8–7.0, and K_{KA}^{H} was therefore set in this range. These two values determine n_{KA}, the only unknown left in Eq. 1a. The volume dependence coefficient, f_{KA}^{V}, on the other hand, is set at 1 for the reference state, becomes < 1 as the cells shrink, and becomes > 1 as they swell. The value of the rate constant k_{KA} was derived from the chosen reference state flux, the K^+ and A^- concentrations, and from the values set for the pH and volume control factors. The values of parameters and initial variables are given in Tables I–III.

Balance of fluxes in the reference state

The equations below list all the flux components considered in the integrated reticulocyte model for the four permeant ions in the system: Na^+, K^+, A, H^+. These are the only equations that differ from those in the fundamental equation set of the RBC model (25).

$$\phi_{Na} = \phi_{Na}^{P} + \phi_{Na}^{L} + \phi_{Na}^{G} + \phi_{Na}^{Co} + \phi_{Na}^{NaH} + \phi_{Na}^{NaA} \quad (2)$$

$$\phi_K = \phi_K^{P} + \phi_K^{L} + \phi_K^{G} + \phi_K^{Co} + \phi_K^{KA} \quad (3)$$

$$\phi_A = \phi_A^{G} + \phi_A^{Co} + \phi_A^{HA} + \phi_A^{KA} + \phi_A^{NaA} \quad (4)$$

$$\phi_H = \phi_H^{G} + \phi_H^{HA} + \phi_H^{NaH} \quad (5)$$

Table III. Variables of the Reticulocyte Model, Option 1, in the Reference State

	Cell Amounts	Concentrations		Other Variables*	
		Cell	Medium		
	mmol/loc	*mmol/lcw*	*mM*		
Na	8.80	10.00	144.14	V_W	0.88
K	123.20	140.00	5.00	V/V	1.13
A	83.60	95.00	145.00	Hct	0.10
H		$6.08.10^{-8}$	$3.98.10^{-8}$	MCHC	30.1
Hb	5.27	5.99		E(mV)	−10.00
X	37.36	42.46		Density	1.080
Mg	2.50	2.84		r_A	1.53
B			10.00	r_H	1.53
HB			5.86	f_{Hb}	2.31
				n_{Hb}	−3.66
				pH^c	7.216
				pH^m	7.400

Options 2 and 3 have the same variable values in the reference state with the following exceptions:

Variable	Option 2	Option 3
E(mV)	−11.29	−11.29
C_H^c	—	$5.76.10^{-8}$
r_H	—	1.45
n_{Hb}	—	−3.9
pH^c	—	7.24

The table also lists the "standard" Hct and medium concentrations used before experimental perturbations. Differences in variable values for options 2 and 3 are given at the bottom of the table. Variable values in the reference state were set or derived as explained in Computation Strategy (Appendix).
* Units as in Glossary.

The superscripts P, L, G, Co, HA, KA, NaA, and NaH designate all the transporters considered in the reticulocyte model; these are, respectively, the Na^+ pump, low saturation carriers, electrodiffusional pathways, the Na:K:2Cl cotransport, the Jacobs–Stewart mechanism, all as defined for the integrated RBC model (25), and three transporters specific to the reticulocyte: the K:Cl cotransport (K:A), the Na:Cl cotransport (Na:A), and the Na^+:H^+ exchange (Na:H).

The Na^+ pump

The influx of K^+ through the pump has to be at least as large as the K^+ efflux through the cotransporter. For consistency with the RBC model, and to allow for future modeling of the maturation process from reticulocyte to RBC, the minor carrier and electrodiffusional flux components of the mature cell were retained in the reticulocyte model. Changes in passive fluxes during maturation can then be modeled simply by inserting decay rate constants for specific reticulocyte flux components. The sum of all passive K^+ efflux components sets the precise size of the compensatory K^+ influx through the pump. The constant Na^+/K^+ stoichiometry of the pump then determines the value of the active Na^+ efflux linked to the required K^+ influx. This, in turn, determines the maximal size of the passive Na^+ influx through all Na^+ transporters in the reference state. The kinetics defined for the Na^+ pump were given above in D10. Reverse fluxes, originally defined to prevent violation of thermodynamic constraints in certain simulations, were retained although they had no direct relevance to the studies reported here.

The Na^+ transporters

Each of the options outlined above requires a different computing strategy for the reference state. In option 1, potential-driven A^- entry, the transmembrane A^- and proton concentration ratios are equal, but the membrane potential must be depolarized relative to the A^- equilibrium potential. In option 2, Na:A cotransport, the ratios are the same and the membrane potential is at the A^- equilibrium potential, as in mature RBCs. In option 3, A^- entry driven by a proton gradient, the membrane potential is again at the A^- equilibrium potential, but the concentration ratios of A^- and protons are now different.

Cell water

The measured mean MCHC is ~ 340 g Hb/liter cells for RBCs, and 300 g Hb/liter cells for reticulocytes (1, 2, 4, 5). We assumed a value of 1,090 g/loch for the mean density of normal RBCs. If we neglect the volume and weight of the membrane and the departure from unity of the water density, the resulting volume of cell water per liter cells for RBCs is 1.090 − 0.340 = 0.750 liters/loc. Hb therefore occupies a volume of 0.25 liters/loc from which we derive a value of 0.250/0.340 = 0.735 ml/g for the specific volume of Hb, which compares well with previous estimates of 0.75 for the partial specific volume of Hb (66). Hence the volume occupied by 300 g Hb, as in 1 liter of reticulocytes, is 0.22 liters. Cell water in the reference state was therefore set at 0.78 liters/loc. These values give a mean density of 1,080 g/loc for reticulocytes. The volume of reticulocytes associated with 340 g Hb is 1.13 liters. This volume will contain the same number of reticulocytes as that in 1 liter of mature RBCs, and represents the volume of reticulocytes relative to that of an equal number of RBCs in the reference steady state ("Relative cell volume" in the ordinate of figures).

Computation of the reference steady state (RS)

The sequence of computations followed for each option is as follows:
Option 1: Potential driven A^- entry
1. Set the values of ϕ_K^{KA}, ϕ_K^G, ϕ_K^L, ϕ_{Na}^L, and E.
2. $\phi_K^P = -(\phi_K^{KA} + \phi_K^L + \phi_K^G)$
3. $\phi_{Na}^P = -1.5\phi_K^P$
4. $\phi_{Na}^G = -(\phi_{Na}^P + \phi_{Na}^L)$
5. $\phi_A^G = -\phi_A^{KA}$
6. Derive P_A^G and P_{Na}^G from the corresponding flux equations for ϕ_A^G and ϕ_{Na}^G.

In this option, the membrane potential (E) has to be set depolarized relative to the A^- equilibrium potential, to generate a driving force for net A^- influx via ϕ_A^G. The net flux through the Jacobs–Stewart mechanism in the reference state is zero, and the A^- and H^+ concentration ratios (r_A and r_H) are equal. The Na:A cotransport and the Na:H exchanger are inactive.

Option 2: Na:A cotransport

1. Set ϕ_K^{KA}, ϕ_K^G, ϕ_K^L, ϕ_{Na}^L, and P_A^G.
2. $\phi_K^P = -(\phi_K^{KA} + \phi_K^L + \phi_K^G)$
3. $\phi_{Na}^P = -1.5 \cdot \phi_K^P$
4. $\phi_A^{NaA} = -\phi_K^{KA}$
5. $\phi_{Na}^G = -(\phi_{Na}^{NaA} + \phi_{Na}^P + \phi_{Na}^L)$
6. Derive P_{Na}^G from ϕ_{Na}^G.

In this option, as in RBCs, the reference state membrane potential is at the A^- equilibrium potential, and $r_A = r_H$. The Na:H exchanger is inactive. The Na:A cotransport was assumed electroneutral and its kinetics were defined by:

$$\phi_A^{NaA} = \phi_{Na}^{NaA} = k_{NaA}(C_{Na}^m C_A^m - C_{Na}^c C_A^c) \quad (6)$$

where k_{NaA} is the rate constant of the Na:A cotransport.

Option 3: Na:H exchange coupled to H:A through Jacobs–Stewart mechanism

1. Set ϕ_K^{KA}, ϕ_K^G, ϕ_K^L, ϕ_{Na}^L, and P_A^G.
2. $\phi_K^P = -(\phi_K^{KA} + \phi_K^L + \phi_K^G)$
3. $\phi_{Na}^P = -s \cdot \phi_K^P$

4. $\phi_{Na}^{NaH} = -\phi_{K}^{KA}$; $\phi_{H}^{NaH} = -\phi_{Na}^{NaH}$
5. $\phi_{H}^{HA} = -\phi_{H}^{NaH}$
6. $C_H^c = [C_A^m \cdot C_H^m - (\phi_H^{HA}/k_{HA})]/C_A^c$
7. $\phi_{Na}^{G} = -(\phi_{Na}^{NaH} + \phi_{Na}^{P} + \phi_{Na}^{L})$
8. Derive P_{Na}^{G} from ϕ_{Na}^{G}.

Here r_A is at electrochemical equilibrium, but $r_H \neq r_A$. It is the proton gradient generated by the Na:H exchanger that secondarily drives the compensatory influx of A^- through the Jacobs–Stewart path. The Na:A cotransport is inactive. The Na:H countertransport was defined electroneutral:

$$\phi_H^{NaH} = -\phi_{Na}^{NaH} = k_{NaH}(C_{Na}^m \cdot C_H^c - C_{Na}^c \cdot C_H^m) \quad (7)$$

where k_{NaH} is the rate constant of the Na:H exchange. In considering a hypothetical Na:H exchanger in reticulocytes, simulations were performed either with kinetic characteristics as described in other cells (40–42, 46), using a pH_i dependence factor similar to that defined in Eq. 1a for the K:Cl cotransport or, for comparison, without pH_i dependence.

Acknowledgments

We wish to thank the Wellcome Trust of Great Britain and the National Institutes of Health (grants HL-28018 and HL-21016) for funds.

References

1. Killmann, S. A. 1964. On the size of normal human reticulocytes. *Acta Med. Scand.* 176:529–533.

2. Rapoport, S., G. M. Guest, and M. Wing. 1944. Size, hemoglobin content, and acid-soluble phosphorus of erythrocytes of rabbits with phenylhydrazine-induced reticulocytosis. *Proc. Soc. Exp. Biol. Med.* 57:334–347.

3. Brecher, G., and F. Stohlman, Jr. 1961. Reticulocyte size and erythropoietic stimulation. *Proc. Soc. Exp. Biol. Med.* 107:887–891.

4. Borsook, H., J. R. Lingrel, J. L. Scaro, and R. L. Milette. 1962. Synthesis of haemoglobin in relation to the maturation of erythroid cells. *Nature (Lond.).* 196:347–350.

5. Clarkson, D. R., and E. M. Moore. 1976. Reticulocyte size in nutritional anemias. *Blood.* 48:669–677.

6. Bernstein, R. E. 1959. Alterations in metabolic energetics and cation transport during aging of red cells. *J. Clin. Invest.* 38:1572–1586.

7. Wiley, J. S., and C. C. Shaller. 1977. Selective loss of calcium permeability on maturation of reticulocytes. *J. Clin. Invest.* 59:1113–1119.

8. Panet, R., and H. Atlan. 1980. Characterization of a potassium carrier in rabbit reticulocyte cell membrane. *J. Membr. Biol.* 52:273–280.

9. Brugnara, C., H. F. Bunn, and D. C. Tosteson. 1986. Regulation of erythrocyte cation and water content in sickle cell anemia. *Science (Wash. DC).* 232:388–390.

10. Brugnara, C., and D. C. Tosteson. 1987. Inhibition of K transport by divalent cations in sickle erythrocytes. *Blood.* 70:1810–1815.

11. Brugnara, C., A. S. Kopin, H. F. Bunn, and D. C. Tosteson. 1985. Regulation of cation content and cell volume in erythrocytes from patients with homozygous hemoglobin C disease. *J. Clin. Invest.* 75:1608–1617.

12. Canessa, M., M. E. Fabry, N. Blumenfeld, and R. L. Nagel. 1987. Volume-stimulated, Cl^--dependent K^+ efflux is highly expressed in young human red cells containing normal hemoglobin or HbS. *J. Membr. Biol.* 97:97–105.

13. Lauf, P. K., and B. E. Theg. 1980. A chloride dependent K^+ flux induced by N-ethylmaleimide in genetically low K^+ sheep and goat erythrocytes. *Biochem. Biophys. Res. Commun.* 92:1422–1428.

14. Lauf, P. K., N. C. Adragna, and R. P. Garay. 1984. Activation by N-ethylmaleimide of a latent K^+-Cl^- flux in human red blood cells. *Am. J. Physiol.* 246:C385–C390.

15. Lauf, P. K., R. Garay, and N. C. Adragna. 1982. *N*-Ethylmaleimide stimulates chloride-dependent K^+ but not Na^+ fluxes in human red cells. *J. Gen. Physiol.* 80:19*a* (Abstr.)

16. Duhm, J. 1987. Furosemide-sensitive K^+ (Rb^+) transport in human erythrocytes: modes of operation, dependence on extracellular and intracellular Na^+, kinetics, pH dependency and the effect of cell volume and n-ethylmaleimide. *J. Membr. Biol.* 98:15–32.

17. Kaji, D., and J. Amblard. 1986. Volume sensitive K transport in human erythrocytes. *J. Gen. Physiol.* 88:719–738.

18. Sachs, J. R. 1988. Volume-sensitive K influx in human red cell ghosts. *J. Gen. Physiol.* 92:685–711.

19. Berkowitz, L. R., and E. P. Orringer. 1987. Cell volume regulation in hemoglobin CC and AA erythrocytes. *Am. J. Physiol.* 252:C300–C306.

20. Brugnara, C., T. V. Ha, and D. C. Tosteson. 1988. Properties of K^+ transport in resealed human erythrocyte ghosts. *Am. J. Physiol.* 255:C346–C356.

21. Brugnara, C., and D. C. Tosteson. 1987. Cell volume, K transport, and cell density in human erythrocytes. *Am. J. Physiol.* 252:C269–C276.

22. Hall, A. C., and J. C. Ellory. 1986. Evidence for the presence of volume-sensitive KCl transport in 'young' human red cells. *Biochim. Biophys. Acta.* 858:317–320.

23. Canessa, M., M. E. Fabry, and R. L. Nagel. 1987. Deoxygenation inhibits the volume-stimulated, Cl^--dependent K^+ efflux in SS and young AA cells. A cytosolic Mg^{2+} modulation. *Blood.* 70:1861–1866.

24. Canessa, M., A. Spalvins, and R. L. Nagel. 1986. Volume-dependent and NEM-stimulated K^+, Cl^- transport is elevated in oxygenated SS, SC and CC human red cells. *FEBS (Fed. Eur. Biochem. Soc.) Lett.* 200:197–202.

25. Lew, V. L., and R. M. Bookchin. 1986. Volume, pH and ion content regulation in human red cells: analysis of transient behavior with an integrated model. *J. Membr. Biol.* 92:57–74.

26. Hunter, M. J. 1977. Human erythrocyte anion permeabilities measured under conditions of net charge transfer. *J. Physiol. (Lond.).* 268:35–49.

27. Cabantchik, Z. I., and A. Rothstein. 1972. The nature of the membrane sites controlling anion permeability of human red blood cells as determined by studies with disulfonic stilbene derivatives. *J. Membr. Biol.* 10:311–330.

28. Gunn, R. B., M. Dalmark, D. C. Tosteson, and J. O. Wieth. 1973. Characteristics of chloride transport in human red blood cells. *J. Gen. Physiol.* 61:185–206.

29. Fortes, P. A. G. 1977. Anion movements in red blood cells. *In* Membrane Transport in Red Cells. J. C. Ellory and V. L. Lew, editors. Academic Press, New York. 175–195.

30. Jennings, M. L. 1985. Kinetics and mechanism of anion transport in red blood cells. *Annu. Rev. Physiol.* 47:519–533.

31. Knauf, P. A., G. F. Fuhrmann, S. Rothstein, and A. Rothstein. 1977. The relationship between anion exchange and net anion flow across the human red blood cell membrane. *J. Gen. Physiol.* 69:363–386.

32. Frohlich, O. 1984. Relative contributions of the slippage and tunneling mechanisms to anion net efflux from human erythrocytes. *J. Gen. Physiol.* 84:877–893.

33. Chipperfield, A. R. 1980. An effect of chloride on (Na + K) cotransport in human red blood cells. *Nature (Lond.).* 286:281–282.

34. Haas, M., and B. Forbush III. 1986. [^{3}H]Bumetanide binding to duck red cells: correlation with inhibition of (Na + K + 2Cl) co-transport. *J. Biol. Chem.* 261:8434–8441.

35. Haas, M., and T. J. McManus. 1985. Effect of norepinephrine on swelling-induced potassium transport in duck red cells. Evidence against a volume-regulatory decrease under physiological conditions. *J. Gen. Physiol.* 85:649–667.

36. McManus, T. J., M. Haas, L. C. Starke, and C. Y. Lytle. 1985. The duck red cell model of volume-sensitive chloride-dependent cation transport. *Ann. NY Acad. Sci.* 456:183–186.

37. Kregenow, F. M. 1977. Transport in avian red cells. *In* Membrane Transport in Red Cells. J. C. Ellory and V. L. Lew, editors. Academic Press, New York. 383–426.

38. Flatman, P. W. 1983. Sodium and potassium transport in ferret red cells. *J. Physiol. (Lond.)*. 341:545–557.

39. Bookchin, R. M., O. E. Ortiz, and V. L. Lew. 1990. Evidence for a direct reticulocyte origin of dense red cells in sickle cell anemia. *J. Clin. Invest.* 86:113–124.

40. Aronson, P. S. 1985. Kinetic properties of the plasma membrane Na^+-H^+ exchanger. *Annu. Rev. Physiol.* 47:545–560.

41. Grinstein, S., and A. Rothstein. 1986. Mechanisms of regulation of the Na^+/H^+ exchanger. *J. Membr. Biol.* 90:1–12.

42. Escobales, N., and M. Canessa. 1986. Amiloride-sensitive Na^+ transport in human red cells: evidence for a Na/H exchange system. *J. Membr. Biol.* 90:21–28.

43. Escobales, N., and M. Canessa. 1985. Ca^{2+}-activated Na^+ fluxes in human red cells: amiloride sensitivity. *J. Biol. Chem.* 260:11914–11923.

44. Jacobs, M. H., and D. R. Stewart. 1947. Osmotic properties of the erythrocyte. XII. Ionic and osmotic equilibria with a complex external solution. *J. Cell. Comp. Physiol.* 30:79–103.

45. Jacobs, M. H., and D. R. Stewart. 1942. The role of carbonic anhydrase in certain ionic exchanges involving the erythrocyte. *J. Gen. Physiol.* 25:539–552.

46. Aronson, P. S., J. Nee, and M. A. Suhm. 1982. Modifier role of internal H^+ in activating the Na^+-H^+ exchanger in renal microvillus membrane vesicles. *Nature (Lond.)*. 299:161–163.

47. Freeman, C. J., R. M. Bookchin, O. E. Ortiz, and V. L. Lew. 1987. K-permeabilized human red cells lose an alkaline, hypertonic fluid containing excess K over diffusible anions. *J. Membr. Biol.* 96:235–241.

48. Lew, V. L., H. G. Ferreira, and T. Moura. 1979. The behaviour of transporting epithelial cells. I. Computer analysis of a basic model. *Proc. R. Soc. Lond. Series B* 206:53–83.

49. Lew, V. L., and L. A. Beauge. 1979. Passive cation fluxes in the red cell membranes. *In* Transport Across Biological Membranes. Vol. II. G. Giebisch, D. C. Tosteson, and H. H. Ussing, editors. Springer-Verlag, Berlin. 85–115.

50. Serjeant, G. R., B. E. Serjeant, and P. F. Milner. 1969. The irreversibly sickled cell: a determinant of haemolysis in sickle cell anaemia. *Br. J. Haematol.* 17:527–533.

51. Fabry, M. E., L. Benjamin, C. Lawrence, and R. L. Nagel. 1984. An objective sign in painful crisis in sickle cell anemia. The concomitant reduction of high density red cells. *Blood.* 64:559–563.

52. Gardos, G. 1958. The function of calcium in the potassium permeability of human erythrocytes. *Biochim. Biophys. Acta.* 30:653–654.

53. Eaton, J. W., T. D. Skelton, H. S. Swofford, C. E. Koplin, and H. S. Jacob. 1973. Elevated erythrocyte calcium in sickle cell disease. *Nature (Lond.)*. 246:105–106.

54. Palek, J. 1973. Calcium accumulation during sickling of haemoglobin S red cells. *Blood.* 42:988–1000.

55. Glader, B. E., and D. G. Nathan. 1978. Cation permeability alterations during sickling. Relation to cation composition and cellular hydration of irreversibly sickled cells. *Blood.* 51:983–989.

56. Bookchin, R. M., O. E. Ortiz, and V. L. Lew. 1987. Activation of calcium-dependent potassium channels in deoxygenated sickled red cells. *In* Pathophysiological Aspects of Sickle Cell Vaso-Occlusion. R. L. Nagel, editor. Alan R. Liss, Inc., New York. 193–200.

57. Clark, M. R., J. C. Guatelli, A. T. White, and S. B. Shohet. 1981. Study on dehydrating effect of the red cell Na^+/K^+-pump in nystatin-treated cells with varying Na^+ and water contents. *Biochim. Biophys. Acta.* 646:422–432.

58. Brugnara, C., T. V. Ha, and D. C. Tosteson. 1989. Acid pH induces formation of dense cells in sickle erythrocytes. *Blood.* 74:487–495.

59. Bertles, J. F., and P. F. A. Milner. 1968. Irreversibly sickled erythrocytes. A consequence of the heterogeneous distribution of hemoglobin types in sickle cell anemia. *J. Clin. Invest.* 47:1731–1741.

60. Lew, V. L., A. Hockaday, M. I. Sepulveda, A. P. Somlyo, A. V. Somlyo, O. E. Ortiz, and R. M. Bookchin. 1985. Compartmentalization of sickle cell calcium in endocytic inside-out vesicles. *Nature (Lond.)*. 315:586–589.

61. Bookchin, R. M., O. E. Ortiz, A. V. Somlyo, A. P. Somlyo, M. I. Sepulveda, A. Hockaday, and V. L. Lew. 1985. Calcium-accumulating inside-out vesicles in sickle cell anemia red cells. *Trans. Assoc. Am. Physiol.* 98:10–20.

62. Ortiz, O. E., R. M. Bookchin, and V. L. Lew. 1988. A new method to measure the distribution of diffusional chloride (Cl) permeabilities in the red cell populations reveals a Ca^{2+}-sensitive Cl permeability in sickle cell anemia reticulocytes. *Clin. Res.* 36:415A. (Abstr.)

63. Dalmark, M. 1975. Chloride and water distribution in human red cells. *J. Physiol. (Lond.)*. 250:65–84.

64. Cass, A., and M. Dalmark. 1973. Equilibrium dialysis of ions in nystatin-treated cells. *Nature (Lond.)*. 244:47–49.

65. Freedman, J. C., and J. F. Hoffman. 1979. Ionic and osmotic equilibria of human red blood cells treated with nystatin. *J. Gen. Physiol.* 74:157–185.

66. Bureau, M., and R. Banerjee. 1976. Structure-volume relationships in hemoglobin: a densitometric and dilatometric study of the oxy leads to deoxy transformation. *Biochimie (Paris)*. 58:403–407.